Algal Research 72 (2023) 103131

Contents lists available at ScienceDirect

Algal Research

journal homepage: www.elsevier.com/locate/algal

Pyruvate orthophosphate dikinase is required for the acclimation to high bicarbonate concentrations in *Phaeodactylum tricornutum*

Teng Huang [a,c], Fan Hu [b], Yufang Pan [a], Chenjie Li [a,c], Hanhua Hu [a,*]

[a] Key Laboratory of Algal Biology, Institute of Hydrobiology, Chinese Academy of Sciences, Wuhan 430072, China
[b] School of Foreign Languages, China University of Geosciences, Wuhan 430074, China
[c] University of Chinese Academy of Sciences, Beijing 100049, China

ARTICLE INFO

Keywords:
C_4 metabolism
Diatom
High bicarbonate
Phaeodactylum tricornutum
Pyruvate orthophosphate dikinase

ABSTRACT

The model marine diatom *P. tricornutum* possesses efficient CO_2-concentrating mechanisms (CCMs) involving the bicarbonate transport and the rapid inter-conversion of HCO_3^- and CO_2, and it has a complete set of enzymes essential for biochemical CCM C_4 pathway. However, the role of potential C_4 pathway in the diatom is still controversial. Based on the analysis of previously published proteome and transcriptome data in *P. tricornutum*, the expression of pyruvate orthophosphate dikinase (PPDK), a key enzyme generating the primary acceptor for bicarbonate fixation in C_4 pathway, was upregulated in long-term high CO_2-selected populations. In our study, *P. tricornutum PPDK* (*PtPPDK*) transcript abundance was higher with short-term treatment of high $NaHCO_3$ concentrations and overexpression of *PtPPDK* resulted in a cell density increase of 5–16 % from day 2 to 8. Knockdown (KD) or knockout of *PtPPDK* inhibited the growth and the maximal photosystem II electron transport rate, and the inhibited growth became more and more evident with the increasing $NaHCO_3$ concentration from 1 to 8 mM in *PtPPDK* KD lines. Furthermore, elevating $NaHCO_3$ from 1 to 16 mM dramatically decreased the cell density both in wild-type and *PtPPDK* mutants, suggesting that 1 mM $NaHCO_3$ is enough for the photosynthesis carbon assimilation. PtPPDK was localized in the plastid stroma by eGFP fusion protein analysis at 2 mM $NaHCO_3$, while PtPPDK-eGFP fluorescence was observed both in the stroma and periplasmic space at higher $NaHCO_3$. It is suggested that PPDK is necessary for consuming excessive inorganic carbon (C_i) both from the plastid and extracellular environment to maintain pH homeostasis, indicating a potential function of adapting to high C_i concentrations.

1. Introduction

Diatoms, operating very efficient photosynthesis, are responsible for up to 40 % of the primary production in oceans and thus are crucial for the global carbon cycle [1]. However, the dissolved inorganic carbon (DIC) in seawater (~2 mM) corresponds to a much lower concentration of CO_2 (10–15 μM at pH 8.2) [2] than the value of CO_2 half-saturation constant (23–68 μM) of ribulose-1,5-bisphosphate carboxylase/oxygenase (RubisCO) in diatoms [3]. To overcome carbon limitation of photosynthesis, diatoms as well as many other phytoplankton possess CO_2-concentrating mechanisms (CCMs) that elevate the CO_2 concentration in the proximity of RubisCO especially in a CO_2-limited environment [1,4].

Two main types of CCMs, biophysical and/or biochemical, are known in diatoms [5]. Biophysical CCMs involve active transport of CO_2 and/or HCO_3^- across biological membranes, coupled with interconversion between CO_2 and HCO_3^- which is catalyzed by carbonic anhydrases (CAs) [6,7]. For instance, SLC4 HCO_3^- transporters and their homologous encoding genes have been reported in *Phaeodactylum tricornutum* [7] and *Thalassiosira pseudonana* [8]. Diatoms possess numerous CAs from common (α, β, γ) and unusual (δ, ζ) families, and some of them in *T. pseudonana* are extracellular and serve to convert HCO_3^- to CO_2 on the cell surface for CO_2 uptake [9]. In *P. tricornutum*, plastidial CAs, especially those located in the pyrenoid (β-CA, PtCA1 and PtCA2; θ-CA, Pt43233) [6,10], are critical for CCM function and efficiency. Biochemical CCMs, referred to as the C_4-type CCM or C_4 pathway, include the formation of intermediate four-carbon organic molecules, which are accumulated and transported within the cell. Some terrestrial and aquatic plants as well as a few algae are reported to perform C_4 photosynthesis, while the presence of C_4 pathways is less

* Corresponding author.
E-mail address: hanhuahu@ihb.ac.cn (H. Hu).

https://doi.org/10.1016/j.algal.2023.103131
Received 15 January 2023; Received in revised form 5 April 2023; Accepted 2 May 2023
Available online 6 May 2023

certain in diatoms. There is evidence of the presence of C_4 photosynthesis in the marine diatom *Thalassiosira weissflogii* [11], however, there are contradictory results for other diatoms including *P. tricornutum* [12–15].

The functional C_4 CCM requires an additional carboxylation enzyme, typically phosphoenolpyruvate (PEP) carboxylase (PEPC), which catalyzes the carboxylation of PEP with HCO_3^-, thus forming a C_4 compound oxaloacetate (OAA). OAA can be directly decarboxylated by PEP carboxykinase (PEPCK) or reduced to malate or aspartate by malate dehydrogenase or aspartate aminotransferase (AAT). *T. pseudonana* and *P. tricornutum*, two sequenced diatoms, possess all the genes required for C_4-type CCM [8,16]. Two carboxylating enzymes, PEPC1 and PEPC2, are reported to locate in the matrix of the periplastidic compartment and the mitochondria, respectively, in these two diatom species [13,17]. Recently the role of the two PEPCs in the CCMs of *P. tricornutum* have been studied [18], and at least parts of the CCM rely on biochemical bicarbonate fixation catalyzed by PEPC2 in mitochondria. PEP can be converted from pyruvate by pyruvate orthophosphate dikinase (PPDK) and may be able to be transported to mitochondria and the plastid as a substrate for PEPC [18], and the regeneration of PEP from pyruvate by PPDK might be necessary to maintain the potential C_4 cycle. However, PPDK silencing has no significant effect on the inorganic carbon (C_i) acquisition and photosynthetic activity under low HCO_3^- (0–250 μM $NaHCO_3$) conditions [14]. Therefore, the function of PPDK in the potential C_4 pathway is far from clear in *P. tricornutum*. No matter whether there is a potential C_4 pathway in *P. tricornutum* and what function PPDK performs in this C_4 cycle, many studies have been carried out under low CO_2 (< 400 ppmv) and $NaHCO_3$ (< 2 mM) conditions. In fact, according to the published expression data [19–22], besides being upregulated under excessively low CO_2 conditions, PPDK expression is also upregulated under high CO_2 conditions in *P. tricornutum*, indicating a potential function of adapting to high C_i concentrations [19,20]. In this study, *PPDK* knockdown (KD), knockout (KO) and overexpression (OE) strains were generated in *P. tricornutum* to illustrate the role of PPDK under the high DIC condition. In addition, the intracellular distribution of PPDK was observed at different HCO_3^- concentrations by generating PPDK:: GFP fusion proteins to further interpret its function.

2. Materials and methods

2.1. Strain and growth conditions

Phaeodactylum tricornutum CCMP2561 was obtained from the culture collection of the Provasoli-Guillard National Center for Culture of Marine Phytoplankton, Bigelow Laboratory for Ocean Sciences (USA). Algal cells were grown in artificial seawater (AW) enriched with silicate-free f/2 (nitrate concentration was reduced to 500 μM) [23] and the initial cell density was 2×10^5 cells mL^{-1}. For the growth of RNA interference (RNAi) lines, overexpression (OE) lines, and eGFP expression lines, 37.5 μg mL^{-1} zeocin was added to the medium. All the cultures were incubated in constant light (60 μmol photons m^{-2} s^{-1}) at 22 °C, and shaken manually three times a day. AW was prepared according to Harrison et al. [24], and different DIC concentrations were obtained by adding $NaHCO_3$ of various concentrations in the AW. To be specific, $NaHCO_3$ levels were set at 1, 2, 4, 8 and 16 mM in the AW. Accordingly, the concentrations of CO_2 were 15.6, 31.2, 62.3, 124.7 and 249.4 μM, and those of HCO_3^- were 0.94, 1.87, 3.74, 7.49 and 14.97 mM in the culture system (pH 7.7, 22 °C, salinity 30.5). Subsamples were retrieved for cell enumeration using a Malassez chamber and pH values of the culture were measured by pH meter.

2.2. Plasmid construction and transformation

The full-length coding sequence of *P. tricornutum PPDK* (*PtPPDK*, Phatr3_J21988) is 3036 bp in length and encodes 1011 amino acids according to Ensembl database annotations. To generate *PtPPDK* OE vector pPhaT1-PPDK-OE for *P. tricornutum*, the coding region of the gene was amplified using the primers *PPDK_KpnI_Fw* (GGggtaccATGAAGTTTTCTTCAGCT) and *PPDK_XbaI_Rev* (GCtctagaTTACGCCATGGGCGAAGTC) and then inserted into the plasmid pPha-T1 between the *Kpn*I and *Xba*I sites. For the subcellular localization analysis of PtPPDK, the pPhaT1-PPDK-eGFP construct was generated to express C-terminal eGFP fusion proteins in *P. tricornutum* cells. Primers *PPDK_KpnI_Fw* and *PPDK_linker* + *KpnI_Rev* (GGggtaccTCCTCCTCCTCCTCCCCTAGGTCCCGCCATGGGCGAAGTCTTG) were used to amplify the open reading frame (ORF) of *PtPPDK*, and the resulting PCR product was inserted into the *Kpn*I site of pPhaT1-eGFP [25]. For the silencing of *PPDK* in *P. tricornutum*, "long" and "short" fragments were amplified to obtain a hairpin construct [26]. In details, a 250-bp fragment (corresponding to the *PtPPDK* gene sequence from 2355 to 2604 bp) and a 445-bp fragment (corresponding to the *PtPPDK* gene sequence from 2355 to 2799 bp) were amplified from the *P. tricornutum* cDNA, respectively, with the primers *ppdk_fw* (CGgaattcCATGCAGACTGAGGCGATTA, containing an *Eco*RI site) and *ppdk_rv1* (GCtctagaGGTCACTCCTGCAATCTGGT, containing an *Xba*I site), and primers *ppdk_fw* and *ppdk_rv2* (GCtctagaAGCCGAAAGATGAAGCAAGA, containing an *Xba*I site). The fragments were digested with *Eco*RI and *Xba*I and ligated in sense and antisense orientations to the *Eco*RI site of the linearized phir-PtGUS vector, replacing the GUS gene fragments. Plasmid pKS diaCas9_sgRNA_PPDK was generated for *PtPPDK* KO lines using CRISPR/Cas9 method as described by Nymark et al. [27]. Target sites for CRISPR/Cas9 were designed within the *PtPPDK* gene using the PHYTOCRISP-EX web tool (https://www.phytocrispex.biologie.ens.fr/CRISP-Ex/) and a 20 bp guide RNA (PPDK_877: GAAAAGGTTTACGACGAACA) was cloned into the pKS diaCas9_sgRNA vector.

Before being transformed into wild-type *P. tricornutum* by electroporation, the vectors were linearized with *Hpa*I (OE and eGFP vectors) or *Sca*I (RNAi vectors) and then purified with DNA purification kit according to our previous method [25]. Co-transformation of the linearized pPha-T1 (by *Sca*I) and the linearized pKS diaCas9_sgRNA_PPDK (by *Kpn*I) was performed for the generation of KO transformants. OE and eGFP fusion transformants were screened by checking the integration of the *PtPPDK* gene, and RNAi transformants were screened by checking the integration of the *sh ble* gene. DNA from resistant colonies after the transformation of CRISPR/Cas9 construct was extracted, amplified by PCR and sequenced for mutant identification. The eGFP transformants grown to the exponential growth phase in liquid media containing 2 and 8 mM $NaHCO_3$ were observed with a Leica TCS SP8 laser scanning confocal microscope. An excitation wavelength of 488 nm was used for eGFP fluorescence and plastid autofluorescence, detected at 500–550 and 650–690 nm respectively.

2.3. Real-time quantitative PCR (RT-qPCR) and Western blot

To examine the RNA and protein expression of PtPPDK, exponential growth cells were harvested by centrifuging at 3000 rpm for 10 min (4 °C). For RNA extraction, cells were washed with phosphate buffered saline and the cell pellet was immediately frozen in liquid nitrogen. RNA was extracted with RNAiso Plus (Takara, China) according to the manufacturer's instructions, and then converted into cDNA according to protocols provided by HiScript III 1st Strand cDNA Synthesis Kit (+gDNA wiper) (Vazyme, China). RT-qPCR was performed in a LightCycler 480 Real-Time PCR System (Roche, Germany) with the LightCycler 480 SYBR Green I Master (Roche). Primer pair *qPPDK_Fw* (CGCTTACGACTCCTTTCGTC) and *qPPDK_Rev* (CCGTGTTCGTCGTAAACCTT) was used for RT-qPCR of *PtPPDK*, and *PtPPDK* expression was normalized on the housekeeping gene *Histone H4* [28]. Relative quantification of mRNA levels was performed in triplicate on two independent cultures. To observe the relative transcript abundance of *PtPPDK* during the time course in medium with different $NaHCO_3$ concentrations (1, 2, 4, 8, and 16 mM), RNA from wild-type *P. tricornutum* grown for 1, 3, 6 and 12 h at 60 μmol photons m^{-2} s^{-1} was sampled, and

then the light-grown cells were transferred to dark for 12 h (designated as "24 h") and subsequently exposed to light for 6 h (designated as "30 h").

Protein extraction was carried out using Western/IP lysis buffer (Beyotime, China), and the protein concentration was measured with the BCA Protein Concentration Assay Kit (Beyotime). Protein samples were isolated by 12 % SDS-PAGE and then transferred to PVDF membrane. After washing, the membranes were incubated with PtPPDK polyclonal antibody and then with HRP-labeled goat anti-rabbit IgG secondary antibody. The blots were developed by ECL (Millipore, USA), and chemiluminescence was captured on an ImageQuant LAS 4000 mini apparatus (GE Healthcare Life Sciences, UK). Polyclonal antibody of PtPPDK was generated by Genscript Corporation (Nanjing, China) against synthetic peptides GSNSMVSEQEDSKHC.

2.4. Chlorophyll fluorescence measurements

In vivo fluorescence measurements of exponential growth cells (grown to 2–3× 10^5 cells mL^{-1}) were performed at room temperature using a JTS-10 spectrophotometer (Biologic, France). The relative electron transport rates at the given light intensities (35, 75, 120, 230, and 450 μmol photons m^{-2} s^{-1}) were obtained by multiplying photosystem II (PSII) efficiency by the light intensity [29]. Data were treated by non-linear fitting technique using model $P = P_m(1 - e^{-(\alpha Ed/Pm)})$ [30], where P_m is the photosynthetic capacity at saturating irradiance (maximum relative electron transport rate $rETR_m = P_m$ in the absence of photoinhibition), α is the initial linear slope of the best fit curve, and $E_k = rETR_m/\alpha$.

3. Results

3.1. Expression level response of PtPPDK to C_i concentrations

To interpret the putative role of PtPPDK in CCMs of *P. tricornutum*, PtPPDK expression levels at different CO_2 concentrations and different growth phases were analyzed based on previously published proteome and transcriptome data. PtPPDK protein level was significantly upregulated [19] and its transcript abundances ([20]; NCBI Accession: PRJEB34512) were also higher in long-term (8–24 months) high CO_2-selected populations of *P. tricornutum* (Fig. 1a). However, the short-term (2 h ~ 10 days) acclimation to elevated CO_2 (1000–5000 ppmv) and ambient air (400 ppmv) resulted in no significant difference in the relative mRNA levels of *PtPPDK* which were significantly upregulated under extremely low CO_2 concentrations (50–150 ppmv) ([21,31]; NCBI Accession: PRJNA322663) (Fig. 1a). As shown by McCarthy et al. [32], the transcript abundance of *PtPPDK* changed a little from 1 to 42 h and then soared till 66 h, and it tended to increase from 90 to 228 h (Fig. 1b). *PtPPDK* transcript levels were also increased during darkness if not changed ([33,34]; NCBI Accession: PRJNA322663) (Fig. 1a). To observe the response of *PtPPDK* mRNA levels to various $NaHCO_3$ concentrations, wild-type *P. tricornutum* was cultured in medium with 1, 2, 4, 8, and 16 mM $NaHCO_3$, and relative mRNA levels of *PtPPDK* were increased with the elevated $NaHCO_3$ concentration from 1 to 16 mM under light for 1 h and under darkness for 12 h (Fig. 1c). In addition, *PtPPDK* transcript levels at least did not obviously downregulate at higher $NaHCO_3$ conditions (8 and 16 mM) compared with 2 mM $NaHCO_3$ (Fig. 1c). These results indicated that *PtPPDK* might be involved in the long-term adaptation and short-term acclimation to higher Ci.

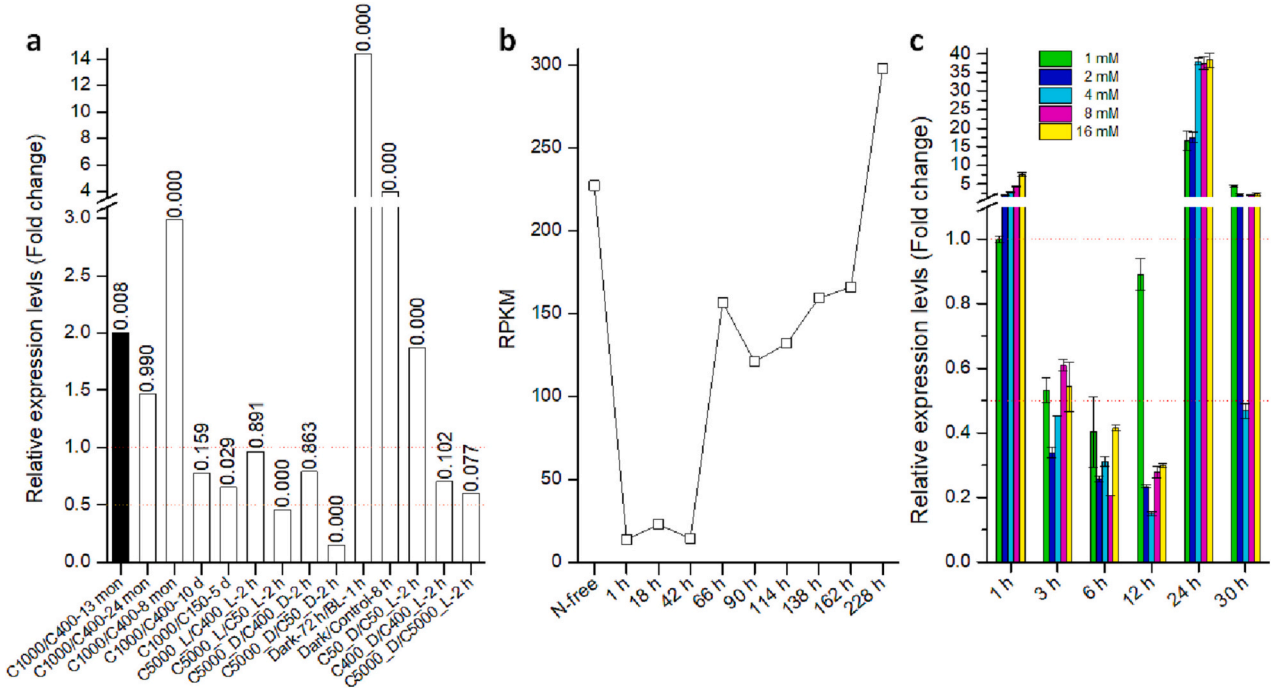

Fig. 1. *P. tricornutum* PPDK expression levels under different growth conditions cited from the published proteome and transcriptome data and in our study. a Protein (black column) and mRNA (white column) fold change at high CO_2 relative to low CO_2 or under darkness relative to light. "C1000", "C400", and "C150" refers respectively to cells grown in 1000, 400, and 150 ppmv CO_2 for *c.* 400 days ("13 mon": [19]), 2 years ("24 mon": [20]), 8 months ("8 mon": NCBI Accession: PRJEB34512), 10 days ("10 d": [31]), or 5 days ("5 d": [21]). "C5000_L (D)", "C400_L (D)", and "C50_L (D)" refers to exponential growth culture with 5000, 400, and 50 ppmv CO_2 for 2 h ("2 h": NCBI Accession: PRJNA322663) at 125 (0) μmol photons m^{-2} s^{-1} after (before) day under 14:10 light dark cycle. "Dark-72 h" and "BL-1 h" refers to cells acclimated to darkness for 72 h and then illuminated with blue light for 1 h [33]. "Control-8 h" and "Dark" refers to cells grown in replete conditions collected at 8 h and under dark treatment for 8 h [34]. P values were indicated above the bars. b Transcript level response to culture time [32]. "N-free" and "1–228 h" refers to "after 2 h of incubation in N-free media" and "1~228 h after transfer of cultures into NO_3^- media". c Wild-type *P. tricornutum* was grown for 1, 3, 6 and 12 h at 60 μmol photons m^{-2} s^{-1} and then the light-grown cells were transferred to dark for 12 h (designated as "24 h") and subsequently exposed to light for 6 h (designated as "30 h"). (For interpretation of the references to colour in this figure legend, the reader is referred to the web version of this article.)

3.2. Growth of PtPPDK mutant and OE lines at high $NaHCO_3$ concentration

To explore the function of PtPPDK in *P. tricornutum*, *PtPPDK* OE, KD and KO lines were generated. Three OE lines (PPDK-OE-1, PPDK-OE-2, and PPDK-OE-5) showing a 17.5, 31.4, and 38.0 fold increase, and three RNAi lines (PPDK-RNAi-1, PPDK-RNAi-2, and PPDK-RNAi-3) showing a 67 %, 75 %, and 86 % reduction, respectively, in transcript levels of *PtPPDK* compared with wild-type were selected for the subsequent analysis (Fig. 2a). A *PtPPDK* KO line (PPDK-Cas9–4) generated by CRISPR-Cas9 technology showed a 4-bp deletion in the target site of *PtPPDK* (Fig. 2b). Immunoblot analysis revealed that PtPPDK protein abundance was obviously higher in the three OE lines and lower in the three KD lines, while no band was detected in the KO line (Fig. 2c).

During a 10-day batch culture period with 2 (Fig. 3a) and 4 mM (Fig. 3b) $NaHCO_3$, significantly different growths were observed between the transformants and wild-type from day 6 to 10. At 2 mM $NaHCO_3$, cell densities in the four *PtPPDK* mutants decreased by 19–21 %, 18–24 %, 12–19 % and 17–21 % from day 8 to 10, and increased by 12–17 %, 6–11 % and 5–9 % in the three OE lines (Fig. 3a). At 4 mM $NaHCO_3$, cell densities in the four *PtPPDK* mutants decreased by 8–14 %, 10–18 %, 14–16 % and 19–22 %, respectively from day 4 to 10. Even on day 2, cell densities of two RNAi lines and the KO line were decreased by 22–33 % compared with the wild-type. On the contrary, overexpression of *PtPPDK* enhanced the growth of *P. tricornutum* and resulted in the cell density increase of 5–16 % from day 2 to 8 (Fig. 3b). It is evident that *PtPPDK* lesion inhibits the growth of *P. tricornutum* at high $NaHCO_3$ conditions, and the increased cell biomass is favoured by *PtPPDK* overexpression.

3.3. Growth response of PtPPDK RNAi lines to gradient $NaHCO_3$ concentrations

To further interpret the function of PtPPDK in *P. tricornutum*, two *PtPPDK* KD lines (PPDK-RNAi-1 and PPDK-RNAi-3) and the wild-type were grown in the media with different concentrations of $NaHCO_3$. A significant growth difference became more and more evident with the increasing $NaHCO_3$ concentration from 1 to 8 mM (Fig. 4). In details, cell density of the two RNAi lines was obviously decreased on day 10 for 1 mM (Fig. 4a), from day 8 to 10 for 2 mM (Fig. 4b), from day 6 to 10 for 4 mM (Fig. 4c), and from day 4 to 10 for 8 mM (Fig. 4d). The maximal decrease of 22–45 % in the cell density was observed for 8 mM from day

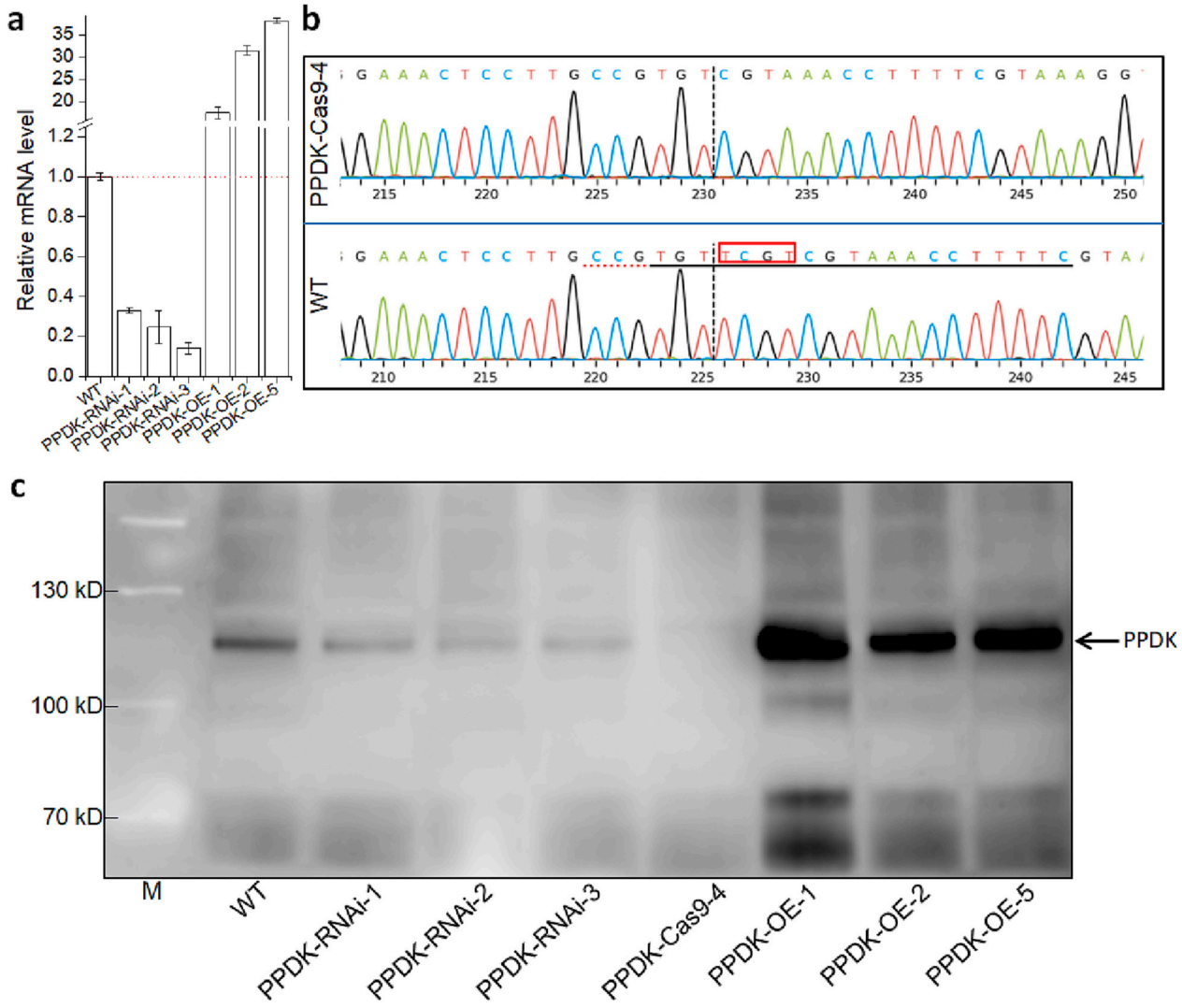

Fig. 2. Expression levels of PtPPDK in *PtPPDK* transformants and sequencing results of *PtPPDK* in *PtPPDK* knockout (KO) line (PPDK-Cas9–4). a Relative mRNA levels of *PtPPDK* in wild-type (WT), RNAi (PPDK-RNAi-1, PPDK-RNAi-2, and PPDK-RNAi-3) and overexpression (OE) lines (PPDK-OE-1, PPDK-OE-2, and PPDK-OE-5). b Sequences of fragment deletions in the *PtPPDK* KO line was aligned with that of WT. c Immunoblotting analysis of PtPPDK protein levels in WT, RNAi, OE, and KO lines.

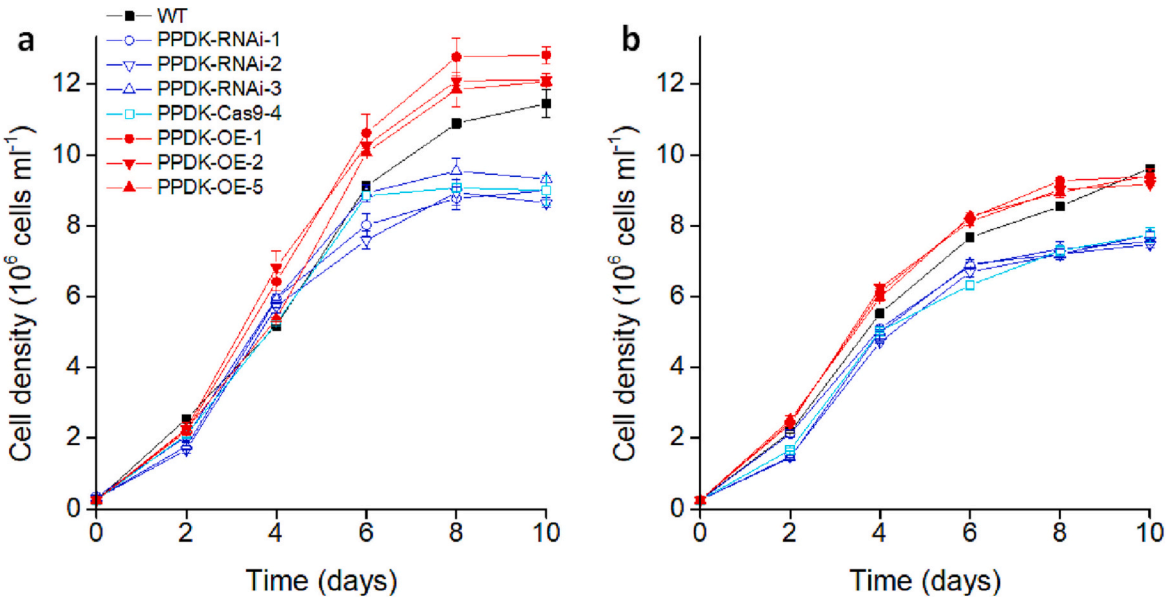

Fig. 3. Growth curves of wild-type (WT), and *PtPPDK* RNAi (PPDK-RNAi-1, PPDK-RNAi-2, and PPDK-RNAi-3), overexpression (OE) (PPDK-OE-1, PPDK-OE-2, and PPDK-OE-5) and knockout (PPDK-Cas9–4) lines cultivated in the medium with 2 (a) and 4 mM $NaHCO_3$ (b). Data are the average of three biological replicates with error bars indicating standard deviations.

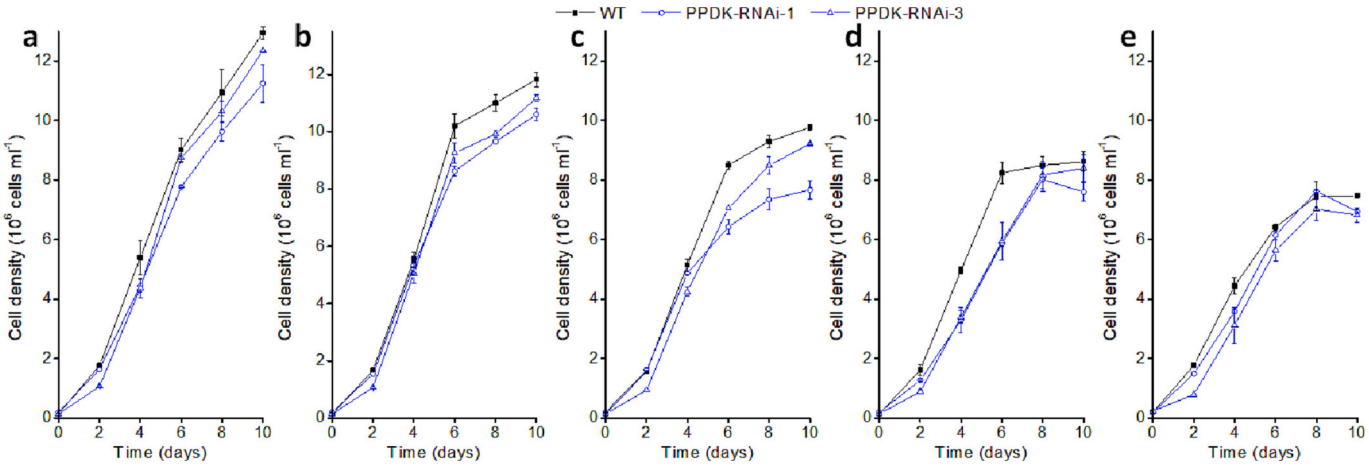

Fig. 4. Growth curves of wild-type (WT) and *PtPPDK* RNAi lines (PPDK-RNAi-1 and PPDK-RNAi-3) cultivated in the medium with 1 (a), 2 (b), 4 (c), 8 (d), and 16 mM (e) $NaHCO_3$. Data are the average of three biological replicates with error bars indicating standard deviations.

2 to 6. Higher $NaHCO_3$ inhibited the growth of not only wild-type but also RNAi lines, and cell density on day 10 decreased by 9 %, 25 %, and 33 % in the wild-type, by 6 %, 32 %, and 32 % in PPDK-RNAi-1, and by 9 %, 25 %, and 33 % in PPDK-RNAi-3 at 2, 4, and 8 mM $NaHCO_3$ relative to 1 mM. A dramatic decrease of 38–45 % in cell density on day 10 was also observed at 16 mM $NaHCO_3$ compared with 1 mM $NaHCO_3$ (Fig. 4e), and there was no obvious difference between the wild-type and RNAi lines, indicating that 16 mM is too high and beyond the regulation of PtPPDK. Fig. 5 shows the pH values of cultures under different $NaHCO_3$ concentrations, and the value was increased by 2.5–2.8 units with the culture time from day 0 to 4, and then slightly decreased by 0.4–0.5 unit from day 4 to 10. However, no significant difference was observed between the RNAi lines and wild-type, suggesting that the growth difference at different $NaHCO_3$ concentrations between the RNAi lines and wild-type can not be attributed to the difference of pH values in the cultures.

3.4. Mutation of PtPPDK decrease photosynthetic capacity of *P. tricornutum*

Corresponding to the decreased growth in *P. tricornutum* by *PtPPDK* knockdown or knockout, mutation of *PtPPDK* also led to a lower relative electron transport rate (rETR) at 2 (Fig. 6a) and 8 mM $NaHCO_3$ (Fig. 6b). In particular, a severe impairment of the photosynthetic capacity was observed in *PtPPDK* mutants at 8 mM $NaHCO_3$ as indicated by the decrease in the maximum relative electron transport rate ($rETR_m$) (Fig. 6b, Table 1). The decreased $rETR_m$ might result from a diminished capacity for carbon fixation. In addition, the $rETR_m$ increased at 8 mM $NaHCO_3$ relative to 2 mM $NaHCO_3$ (Table 1), indicating the increasing photon capture due to the increasing carbon fixation.

3.5. Subcellular localization of PtPPDK at normal and high $NaHCO_3$ concentrations

PtPPDK was predicted to be targeted to the plastid (chloroplast) by TargetP [35] and HECTAR [36], and the former predicted PtPPDK to

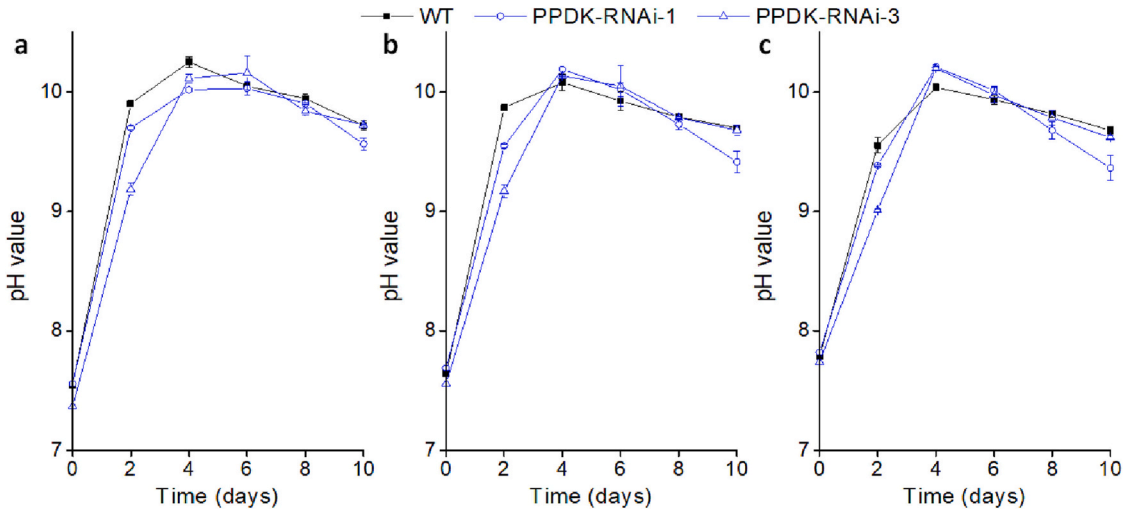

Fig. 5. pH values in the culture of wild-type (WT) and *PtPPDK* RNAi lines (PPDK-RNAi-1 and PPDK-RNAi-3) cultivated in the medium with 1 (a), 2 (b), and 4 mM (c) $NaHCO_3$. Data are the average of three biological replicates with error bars indicating standard deviations.

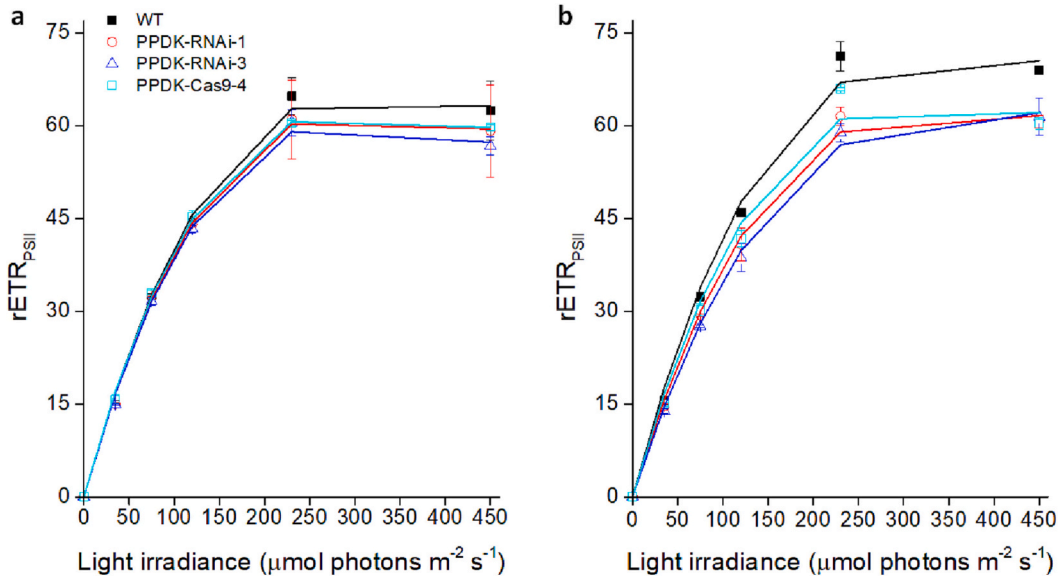

Fig. 6. Photosystem II relative electron transport rate ($rETR_{PSII}$) as a function of the light intensity (35, 75, 120, 230, and 450 μmol photons m^{-2} s^{-1}) in wild-type (WT), two *PtPPDK* RNAi lines (PPDK-RNAi-1 and PPDK-RNAi-3) and a *PtPPDK* knockout line (PPDK-Cas9–4). Experiments were performed on cells grown in the medium with 2 (a) and 8 mM $NaHCO_3$ (b), and the error bars represent ±SD of three biological replicates.

Table 1
Parameters of light-response curves of rETR in wild-type (WT), two PtPPDK RNAi lines (PPDK-RNAi-1 and PPDK-RNAi-3) and a PtPPDK knockout line (PPDK-Cas9–4): initial slope (α, μmol photons $^{-1}$ m^2 s), maximum relative electron transport rate ($rETR_m$), and light saturation coefficient (E_k, μmol photons m^{-2} s^{-1}) (average ± standard deviation, $n = 3$).

	α	$rETR_m$	E_k
2 mM $NaHCO_3$			
WT	0.62 ± 0.07	66.93 ± 3.86	107.95 ± 13.69
PPDK-RNAi-1	0.62 ± 0.06	62.92 ± 3.19	101.48 ± 12.80
PPDK-RNAi-3	0.62 ± 0.07	60.96 ± 3.54	98.32 ± 12.48
PPDK-Cas9–4	0.64 ± 0.05	62.93 ± 2.63	98.32 ± 8.71
8 mM $NaHCO_3$			
WT	0.62 ± 0.08	74.86 ± 5.35	120.74 ± 17.81
PPDK-RNAi-1	0.55 ± 0.06	65.15 ± 3.82	118.45 ± 14.67
PPDK-RNAi-3	0.55 ± 0.04	63.89 ± 2.47	116.16 ± 9.57
PPDK-Cas9–4	0.59 ± 0.09	66.13 ± 5.43	112.08 ± 19.42

have a chloroplast transit peptide (cTP) with a score of 0.5, while the latter with a score of 0.6. However, AsAFind [37], a specific diatom plastid protein prediction program, predicted that the protein was not plastid-localized ("Not plastid, SignalP negative"). PtPPDK was predicted not to contain transmembrane helices by TMHMM Server [38]. To determine the position of PtPPDK in *P. tricornutum*, translational fusion of the *eGFP* gene to the 3′ end of *PtPPDK* was performed. As shown in Fig. 7a, PtPPDK-eGFP fluorescence overlaid with the chlorophyll autofluorescence, clearly demonstrating that the protein was localized in the plastid at normal $NaHCO_3$ concentration. Interestingly, besides in the plastid stroma, green PtPPDK-eGFP fluorescence also appeared around the cell periphery as a ring (Fig. 7b) at the high $NaHCO_3$ concentration (8 mM), indicating that the enzyme was localized in the periplasmic space of *P. tricornutum*.

4. Discussion

Marine diatoms contribute about 20 % of the global primary

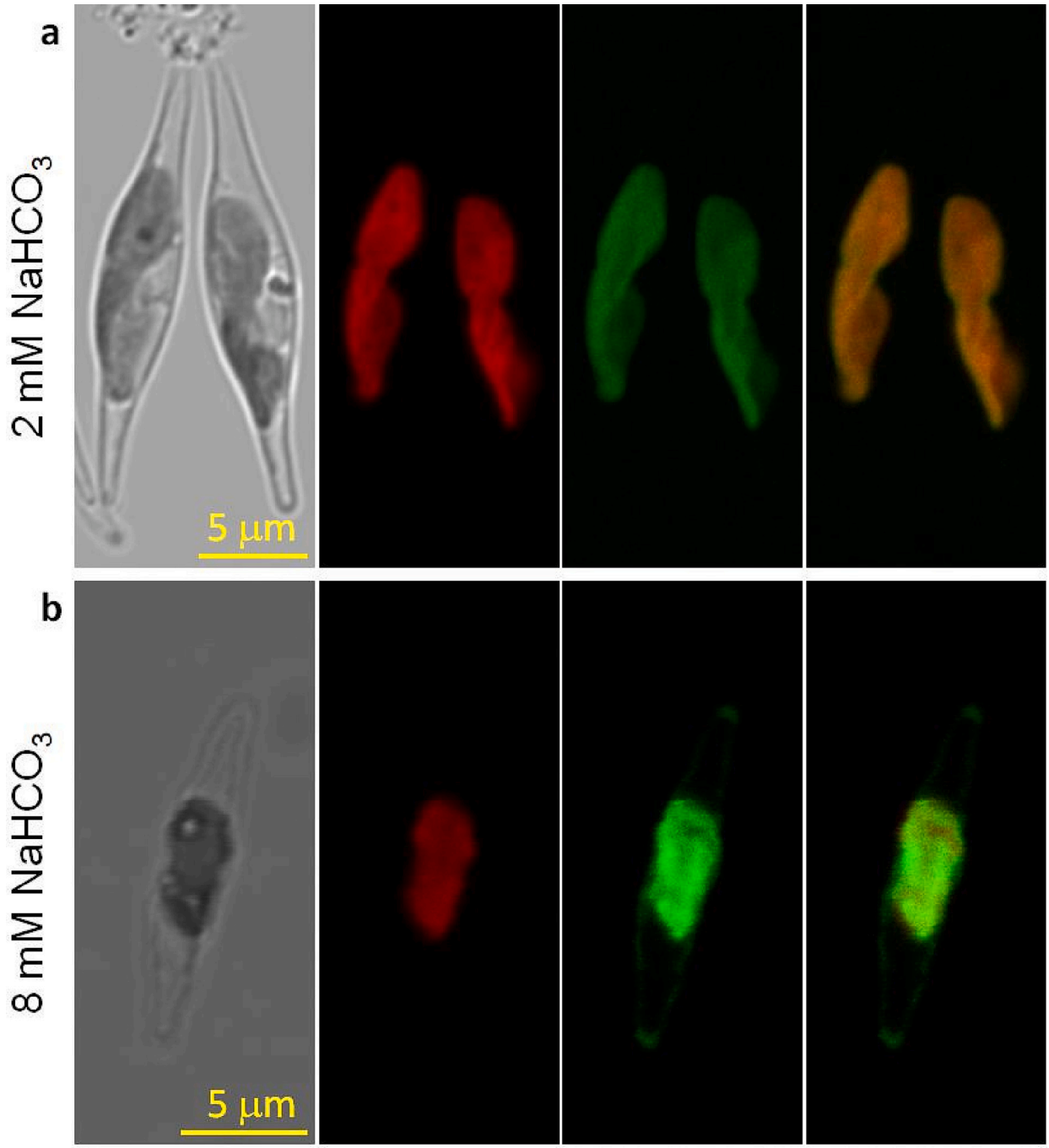

Fig. 7. Fluorescent microscope images of cells expressing PtPPDK-eGFP. From left to right, panels show microscope images of transmitted light, chlorophyll autofluorescence, GFP fluorescence, and a merged image. Experiments were performed on cells grown in the medium with 2 (a) and 8 mM $NaHCO_3$ (b).

productivity [39,40] and rely on CCMs to maintain the productivity at low CO_2 concentrations in the oceans [41]. The model marine diatom *P. tricornutum* possesses efficient CCMs involving the bicarbonate transport by the SLC4 family transporters [7] and the rapid interconversion of HCO_3^- and CO_2 catalyzed by ubiquitous 11 CAs especially in the pyrenoid [6,10]. Furthermore, the role of a potential C_4 pathway for the CCMs in *P. tricornutum* is still controversial. Haimovich-Dayan et al. [14] proposes that the C_4 metabolism does not function in net CO_2 fixation but helps the cells to dissipate excess light energy and maintain the pH homeostasis in *P. tricornutum* under extreme CO_2 limitation, and the intracellular distribution of inorganic carbon fixing enzymes also does not support the presence of a C_4 pathway in the diatom [13]. However, Yu et al. [18] shows that mitochondrial PEPC acts as a component of a biochemical CCM pathway in *P. tricornutum* at low C_i concentrations. PPDK catalyzes the formation of PEP, the initial acceptor for fixation of bicarbonate in the C_4 pathway. Regardless of the presence of C_4 pathway in *P. tricornutum*, the upregulation of *PtPPDK* under extremely low CO_2 concentrations (Fig. 1a) suggests that PtPPDK is involved in the bicarbonate fixation at least. Besides being upregualted under low C_i availability (< 400 ppmv), PtPPDK expression was upregulated in *P. tricornutum* grown under long-term exposures to high CO_2 conditions (Fig. 1a). Our results showed that the *PtPPDK* transcript abundance increased gradually in response to short-term (1 h) treatment of higher concentrations of $NaHCO_3$ (Fig. 1c). Furthermore, PPDK is the only significantly upregulated protein among all C_4-related enzymes [19], though two mitochondrion-localized decarboxylases PEPCK and

ME2 were also transcriptionally upregulated in the long-term (8–24 months) high CO_2-selected *P. tricornutum* cells (Supplemental Fig. S1). In addition, Wu et al. [22] showed that both transcript and protein abundances of PPDK were significantly upregulated at normal CO_2 (400 ppmv) relative to low CO_2 (100 ppmv) for the 7 days' culture. These data all suggested that PPDK might be involved in the adaptation to the high C_i, as indicated by the enhanced growth of *PtPPDK* OE lines and inhibited growth of KO/KD lines at high $NaHCO_3$ (Figs. 3, 4). However, elevating $NaHCO_3$ from 1 to 16 mM dramatically decreased the cell density in *P. tricornutum* both in wild-type and PPDK mutants (Fig. 4), suggesting even 1 mM $NaHCO_3$ is enough for the photosynthesis carbon assimilation. Indeed, in *P. tricornutum* approximately one-third of the DIC transported into the chloroplast is fixed by RubisCO and the rest diffuses as CO_2 into the cytoplasm, where it is recovered by CA-catalyzed hydration to HCO_3^- [42]. The excessive HCO_3^- can combine with PEP provided by PPDK, which is essential for the efficient control of intracellular pH. Haimovich-Dayan et al. [14] considers that C_4 metabolism in *P. tricornutum* does not function in net CO_2 fixation but helps the cells in pH homeostasis. During the PEP formation from pyruvate, ATP is consumed, and thus the futile C_4 cycle in *P. tricornutum* also helps to dissipate excessive energy.

Subcellular localization of key enzymes is critical to a functional C_4 pathway for unicellular algae. The intracellular locations of all enzymes potentially involved in C_4-like carbon fixing pathways in *P. tricornutum* were determined [13]. However, the location of PtPPDK remains uncertain. The full-length protein has a predicted plastid targeting presequence by ChloroP v1.1 (the cleavage site was between the 47th and 48th amino acid residues), while PtPPDK::GFP fusion proteins were observed with a cytosolic location [13]. Contradictorily, the single encoded PPDK regulator protein 1 (RP1-PPDK) was located in the plastid [13]. Thus Ewe et al. [13] supposed that PPDK was dual-targeted in *P. tricornutum*, similar to land plants [43]. In our study, fluorescence of PtPPDK::GFP fusion proteins was observed in the plastid stroma at the normal $NaHCO_3$ concentration, which is consistent with the reported location of RP1-PPDK in Ewe et al. [13]. Stromal PPDK could efficiently catalyze the phosphorylation of pyruvate into PEP, which may be transported to PPC as a substrate for PEPC1 (Fig. 8). Correspondingly, knockdown of PPDK was reported to cause an accumulation of lipids and carbohydrates in *P. tricornutum* [14] due to the decreased consumption of pyruvate by PPDK which induced a metabolic imbalance in the plastid [44].

Under the high $NaHCO_3$ condition, a large amount of HCO_3^- transported by PtSLC4 can be converted into CO_2 by CA around the pyrenoid for photosynthesis. In addition, PPS-localized PPDK provides PEP, which is combined with HCO_3^- by PEPC to produce OAA immediately. OAA can be transported into the mitochondria and then enters the tricarboxylic acid (TCA) cycle or be converted into α-ketoglutarate by AAT to provide carbon skeletons for the amino acid synthesis. A hypothesized working model illustrating the role of PtPPDK in C_i assimilation in *P. tricornutum* was shown in Fig. 8. Anyway the fixed HCO_3^- by PEPC will not be transferred to the plastid for photosynthesis owing to the absence of decarboxylation enzymes in the plastid of *P. tricornutum*. In conclusion, though C_4 pathway does not function due to the lack of the chloroplastic decarboxylase, as a key enzyme of the C_4 pathway PPDK is necessary for consuming excessive C_i both from the plastid and extracellular environment to maintain pH homeostasis or dissipate excessive ATP.

Supplementary data to this article can be found online at https://doi.org/10.1016/j.algal.2023.103131.

CRediT authorship contribution statement

HH, taking responsibility for the integrity of the work as a whole, designed the research, analyzed the data and wrote the manuscript. FH wrote and revised this manuscript. TH, YP and CL performed the

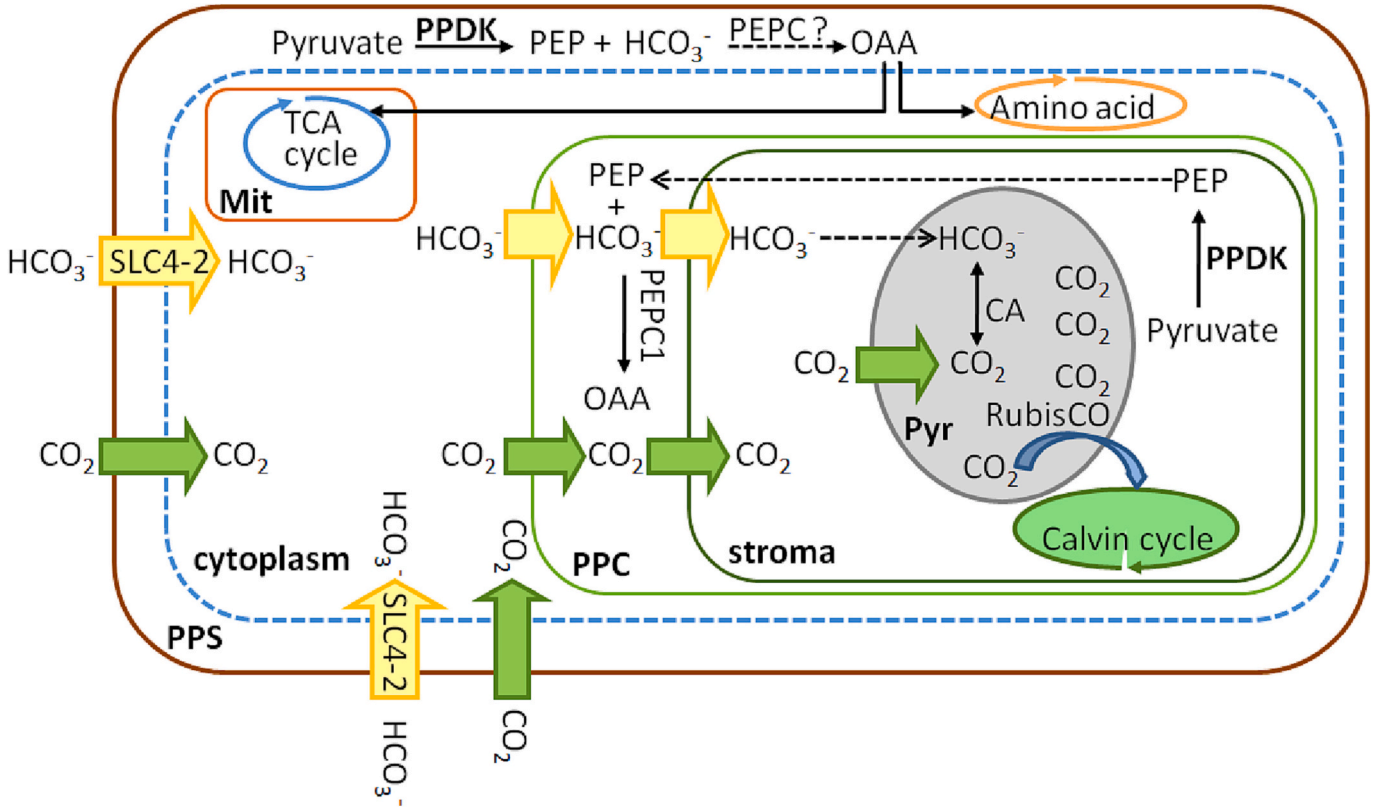

Fig. 8. A hypothesized working model illustrating the role of PtPPDK in bicarbonate fixation in *P. tricornutum*. PPS, periplasmic space; PPC, periplastidal compartment; Pyr, pyrenoid; Mit, mitochondria; CA, carbonic anhydrase; PEP, phosphoenolpyruvate; PEPC, phosphoenolpyruvate carboxylase; PPDK, pyruvate orthophosphate dikinase; OAA, oxaloacetate; RubisCO, ribulose-1,5-bisphosphate carboxylase/oxygenase; SLC4, solute carrier 4.

experiments and analyzed the data.

Statement of informed consent

No conflicts, informed consent, human or animal rights applicable. All authors agree on the authorship and submission of the manuscript for peer review.

Declaration of competing interest

The authors declare that they have no known competing financial interests or personal relationships that could have appeared to influence the work reported in this paper.

Data availability

No data was used for the research described in the article.

Acknowledgement

This work was supported by the National Natural Science Foundation of China (91751117 and 41976119) and International Partnership Program of Chinese Academy of Sciences (Grant No. 075GJHZ2022014MI).

References

[1] K. Roberts, E. Granum, R. Leegood, J. Raven, Carbon acquisition by diatoms, Photosynth. Res. 93 (2007) 79–88.
[2] U. Riebesell, D. Wolf-Gladrow, V. Smetacek, Carbon dioxide limitation of marine phytoplankton growth rates, Nature 361 (1993) 249–251.
[3] J.N. Young, A.M. Heureux, R.E. Sharwood, R.E. Rickaby, F.M. Morel, S. M. Whitney, Large variation in the rubisco kinetics of diatoms reveals diversity among their carbon-concentrating mechanisms, J. Exp. Bot. 67 (2016) 3445–3456.
[4] R. Clement, L. Dimnet, S.C. Maberly, B. Gontero, The nature of the CO2-concentrating mechanisms in a marine diatom, Thalassiosira pseudonana, New Phytol. 209 (2016) 1417–1427.
[5] J.R. Reinfelder, Carbon concentrating mechanisms in eukaryotic marine phytoplankton, Annu. Rev. Mar. Sci. 3 (2011) 291–315.
[6] S. Kikutani, K. Nakajima, C. Nagasato, Y. Tsuji, A. Miyatake, Y. Matsuda, Thylakoid luminal θ-carbonic anhydrase critical for growth and photosynthesis in the marine diatom Phaeodactylum tricornutum, Proc. Natl. Acad. Sci. U. S. A. 113 (2016) 9828–9833.
[7] K. Nakajima, A. Tanaka, Y. Matsuda, SLC4 family transporters in a marine diatom directly pump bicarbonate from seawater, Proc. Natl. Acad. Sci. U. S. A. 110 (2013) 1767–1772.
[8] E.V. Armbrust, J.A. Berges, C. Bowler, B.R. Green, D. Martinez, N.H. Putnam, et al., The genome of the diatom Thalassiosira pseudonana: ecology, evolution, and metabolism, Science 306 (2004) 79–86.
[9] M. Samukawa, C. Shen, B.M. Hopkinson, Y. Matsuda, Localization of putative carbonic anhydrases in the marine diatom, Thalassiosira pseudonana, Photosynth. Res. 121 (2014) 235–249.
[10] M. Tachibana, A.E. Allen, S. Kikutani, Y. Endo, C. Bowler, Y. Matsuda, Localization of putative carbonic anhydrases in two marine diatoms Phaeodactylum tricornutum and Thalassiosira pseudonana, Photosynth. Res. 109 (2011) 205–221.
[11] J.R. Reinfelder, A.M. Kraepiel, F.M. Morel, Unicellular C4 photosynthesis in a marine diatom, Nature 407 (2000) 996–999.
[12] J. Beardall, D. Mukerji, H.E. Glover, I. Morris, The path of carbon in photosynthesis in marine phytoplankton, J. Phycol. 12 (1976) 409–417.
[13] D. Ewe, M. Tachibana, S. Kikutani, A. Gruber, C.R. Bártulos, G. Konert, A. Kaplan, Y. Matsuda, P.G. Kroth, The intracellular distribution of inorganic carbon fixing enzymes does not support the presence of a C4 pathway in the diatom Phaeodactylum tricornutum, Photosynth. Res. 137 (2018) 263–280.
[14] M. Haimovich-Dayan, N. Garfinkel, D. Ewe, Y. Marcus, A. Gruber, H. Wagner, P. G. Kroth, A. Kaplan, The role of C4 metabolism in the marine diatom Phaeodactylum tricornutum, New Phytol. 197 (2013) 177–185.
[15] P.J. McGinn, F.M. Morel, Expression and inhibition of the carboxylating and decarboxylating enzymes in the photosynthetic C4 pathway of marine diatoms, Plant Physiol. 146 (2008) 300–309.
[16] C. Bowler, A.E. Allen, J.H. Badger, J. Grimwood, K. Jabbari, A. Kuo, et al., The phaeodactylum genome reveals the evolutionary history of diatom genomes, Nature 456 (2008) 239–244.
[17] R. Tanaka, S. Kikutani, A. Mahardika, Y. Matsuda, Localization of enzymes relating to C4 organic acid metabolisms in the marine diatom, Thalassiosira pseudonana, Photosynth. Res. 121 (2014) 251–263.
[18] G. Yu, K. Nakajima, A. Gruber, C. Rio Bartulos, A.F. Schober, B. Lepetit, E. Yohannes, Y. Matsuda, P.G. Kroth, Mitochondrial phosphoenolpyruvate carboxylase contributes to carbon fixation in the diatom Phaeodactylum tricornutum at low inorganic carbon concentrations, New Phytol. 235 (4) (2022) 1379–1393.
[19] P. Jin, Y. Ji, Q. Huang, P. Li, J. Pan, H. Lu, Z. Liang, Y. Guo, J. Zhong, J. Beardall, J. Xia, A reduction in metabolism explains the tradeoffs associated with the long-term adaptation of phytoplankton to high CO2 concentrations, New Phytol. 233 (5) (2022) 2155–2167.
[20] P. Jin, J. Wan, Y. Zhou, K. Gao, J. Beardall, J. Lin, J. Huang, Y. Lu, S. Liang, K. Wang, Z. Ma, J. Xia, Increased genetic diversity loss and genetic differentiation in a model marine diatom adapted to ocean warming compared to high CO2, ISME J. 16 (2022) 2587–2598.
[21] J. Levering, C.L. Dupont, A.E. Allen, B.O. Palsson, K. Zengler, Integrated regulatory and metabolic networks of the marine diatom Phaeodactylum tricornutum predict the response to rising CO2 levels, mSystems 2 (1) (2017) e00142-16.
[22] S. Wu, W. Gu, S. Jia, L. Wang, L. Wang, X. Liu, L. Zhou, A. Huang, G. Wang, Proteomic and biochemical responses to different concentrations of CO2 suggest the existence of multiple carbon metabolism strategies in Phaeodactylum tricornutum, Biotechnol. Biofuels 14 (1) (2021) 1–17.
[23] R.R.L. Guillard, Culture of phytoplankton for feeding marine invertebrates, in: W. L. Smith, M.H. Canley (Eds.), Culture of Marine Invertebrate Animals, Plenum Press, New York, 1975, pp. 29–60.
[24] P.J. Harrison, R.E. Waters, F.J.R. Taylor, A broad spectrum artificial seawater medium for coastal and open ocean phytoplankton, J. Phycol. 16 (1) (1980) 28–35.
[25] C. Zhang, H. Hu, High-efficiency nuclear transformation of the diatom Phaeodactylum tricornutum by electroporation, Mar. Genomics 16 (2014) 63–66.
[26] V. De Riso, R. Raniello, F. Maumus, A. Rogato, C. Bowler, A. Falciatore, Gene silencing in the marin ediatom Phaeodactylum tricornutum, Nucleic Acids Res. 37 (2009), e96.
[27] M. Nymark, A.K. Sharma, T. Sparstad, A.M. Bones, P. Winge, A CRISPR/Cas9 system adapted for gene editing in marine algae, Sci. Rep. 6 (2016) 24951.
[28] M. Siaut, M. Heijde, M. Mangogna, A. Montsant, S. Coesel, A. Allen, A. Manfredonia, A. Falciatore, C. Bowler, Molecular toolbox for studying diatom biology in Phaeodactylum tricornutum, Gene 406 (2007) 23–35.
[29] L. Taddei, G.R. Stella, A. Rogato, B. Bailleul, A.E. Fortunato, R. Annunziata, R. Sanges, M. Thaler, B. Lepetit, J. Lavaud, M. Jaubert, G. Finazzi, J.-P. Bouly, A. Falciatore, Multisignal control of expression of the LHCX protein family in the marine diatom Phaeodactylum tricornutum, J. Exp. Bot. 67 (13) (2016) 3939–3951.
[30] T. Platt, C.L. Gallegos, W.G. Harrison, Photinhibition of photosynthesis in natural assemblages of marine phytoplankton, J. Mar. Res. 38 (1980) 687–701.
[31] R. Huang, J. Ding, K. Gao, M.H. Cruz de Carvalho, L. Tirichine, C. Bowler, X. Lin, A potential role for epigenetic processes in the acclimation response to elevated pCO2 in the model diatom Phaeodactylum tricornutum, Front. Microbiol. 9 (2019) 3342.
[32] J.K. McCarthy, S.R. Smith, J.P. McCrow, M. Tan, H. Zheng, K. Beeri, R. Roth, C. Lichtle, U. Goodenough, C.P. Bowler, C.L. Dupont, A.E. Allen, Nitrate reductase knockout uncouples nitrate transport from nitrate assimilation and drives repartitioning of carbon flux in a model pennate diatom, Plant Cell 29 (2017) 2047–2070.
[33] S. König, M. Eisenhut, A. Bräutigam, S. Kurz, A.P.M. Weber, C. Büchel, The influence of a cryptochrome on the gene expression profile in the diatom Phaeodactylum tricornutum under blue light and in darkness, Plant Cell Physiol. 58 (11) (2017) 1914–1923.
[34] M. Matthijs, M. Fabris, T. Obata, I. Foubert, J.M. Franco-Zorrilla, R. Solano, A. R. Fernie, W. Vyverman, A. Goossens, The transcription factor bZIP14 regulates the TCA cycle in the diatom Phaeodactylum tricornutum, EMBO J. 36 (2017) 1559–1576.
[35] O. Emanuelsson, H. Nielsen, S. Brunak, G. von Heijne, Predicting subcellular localization of proteins based on their N-terminal amino acid sequence, J. Mol. Biol. 300 (2000) 1005–1016.
[36] B. Gschloessl, Y. Guermeur, J.M. Cock, HECTAR: a method to predict subcellular targeting in heterokonts, BMC Bioinform. 9 (2008) 393.
[37] A. Gruber, G. Rocap, P.G. Kroth, E.V. Armbrust, T. Mock, Plastid proteome prediction for diatoms and other algae with secondary plastids of the red lineage, Plant J. 81 (2015) 519–528.
[38] A. Krogh, B. Larsson, G. von Heijne, E.L. Sonnhammer, Predicting transmembrane protein topology with a hidden markov model: application to complete genomes, J. Mol. Biol. 305 (2001) 567–580.
[39] P.G. Falkowski, M.E. Katz, A.H. Knoll, A. Quigg, J.A. Raven, O. Schofield, F.J. R. Taylor, The evolution of modern eukaryotic phytoplankton, Science 305 (2004) 354–360.
[40] C.B. Field, M.J. Behrenfeld, J.T. Randerson, P. Falkowski, Primary production of the biosphere: integrating terrestrial and oceanic components, Science 281 (1998) 237–240.
[41] P.D. Tortell, Evolutionary and ecological perspectives on carbon acquisition in phytoplankton, Limnol. Oceanogr. 45 (2000) 744–750.
[42] B.M. Hopkinson, C.L. Dupont, A.E. Allen, F.M.M. Morel, Efficiency of the CO2-concentrating mechanism of diatoms, Proc. Natl. Acad. Sci. U. S. A. 108 (10) (2011) 23830–23837.
[43] K. Parsley, J.M. Hibberd, The arabidopsis PPDK gene is transcribed from two promoters to produce differentially expressed transcripts responsible for cytosolic and plastidic proteins, Plant Mol. Biol. 62 (2006) 339–349.
[44] H. Wagner, T. Jakob, A. Fanesi, C. Wilhelm, Towards an understanding of the molecular regulation of carbon allocation in diatoms: the interaction of energy and carbon allocation, Philos. Trans. R. Soc. B 372 (2017), 20160410.